Fabrication of Nanostructured Poly(3-thiophene methyl acetate) within Poly(vinylidene fluoride) Matrix: New Physical and Conducting Properties

Swarup Manna, Amit Mandal, and Arun K. Nandi*

Polymer Science Unit, Indian Association for the Cultivation of Science, Jadavpur, Calcutta 700 032, India

Received: October 13, 2009; Revised Manuscript Received: January 6, 2010

Nanostructured poly(3-thiophene methyl acetate) (PTMA) within the poly(vinylidene fluoride) (PVDF) matrix is achieved by reactive blending technique under melt-cooled condition. The nanoparticles are almost spherical showing a minimum size with 5% (w/w) PTMA concentration (PTMA5), and they become agglomerated at ≥25% (w/w) PTMA concentration. Different phase separation mechanisms are used to explain the above variation of nanoparticle size. The lower size nanophase in the PTMA5 blend is attributed to spinodal decomposition, while the larger size nanophases are produced from binodal decomposition. The TGA study indicates increasing thermal stability of PVDF in the nanoblends. DSC study shows increasing melting and crystallization temperature of the nanoblends; the former is due to the attractive forces of PTMA nanostructure, and the latter is for the nucleating effect of nanophase PTMA. The long distance, lamellar distance, and amorphous overlayer distance decrease to different extents. The $\pi-\pi^*$ transition band of UV−vis spectra shows a red shift with increasing PTMA concentration, but the photoluminescence spectra of the nanoblends show a blue shift. The former is attributed to intrachain aggregation of PTMA, while the latter is caused from "static excimer" formation at the ground state. PTMA1 and PTMA3 show ∼8 times increase in PL intensity except PTMA5 where interconnectivity between the nanodomains makes the nonradiative decay similar to bulk PTMA. The temperature variation of conductivity indicates a conformational transition of PTMA chain with increasing temperature facilitating better charge transport. The $I-V$ characteristic curves are really interesting; the nanoblends show a negative hysterisis, but PTMA5 shows a memory effect attributed to the electrical bistability originated from the interconnected nanophases arising from spinodal decomposition.

Introduction

Polymer blends with nanometer-scale structure are a new and fascinating area of research because of the origin of new properties suitable for application in advance technologies.[1–7] The high surface area to volume ratio of the nanophase polymer affords an important role in enhancing the physical, thermal, and mechanical properties[7] and also provides a better contact of the nanophases with the matrix polymer.[8,9] It may also influence the chain configuration of the matrix polymer, and hence, the glass transition, crystallization, optical property, etc., may change. Besides, the nanostructure polymer may afford new physical, optical, and electronic properties suitable for sensor, energy research, and biomedical applications.[10–15] Nanofibers of polyaniline have superior performance as chemical and gas sensor due to the larger amount of exposed surface area.[13–15] The field-effect transistor based on nanostructure regioregular poly(3-hexylthiophene) shows good chemical sensing responses.[12] The electrical bistability and nonvolatility has been combined with the conductivity and rectification properties of conducting polymer using network structure of poly(vinylidene-fluoride-*co*-trifluorethylene) [P(VDF-TrFE)] and poly(3-hexylthiophene)(P3HT) blend.[10] Here, the blend structure is macro-phase-separated where the chemical contacts of the two polymers are not good, as there is no specific interaction between the components. In this Article, we report the properties of a new blend of poly(vinylidene fluoride) (PVDF) with nanostruc-

tured poly(3-thiophene methyl acetate) (PTMA) dispersed cocontinuously (i.e., with a diffuse interphase) in the PVDF matrix.

The preparation procedure of nanostructure polymer blend may be divided into three categories: (i) arresting the non-equilibrium morphology produced by high temperature mixing using high shear and compatiblizers,[6,9] (ii) using the self-assembling property of diblock/triblock copolymer in the presence of a component homopolymer where the latter adopts the nanostructure derived from self-assembling of block copolymer,[5,9,16,17] and (iii) a reactive blending procedure for polymers having complementary reactant groups in the chain.[4,7] Among these three procedures, the last one is very effective because the chemical interaction between the nanophase domains and the matrix polymer plays an important role in the stabilization of the nanostructure from the random distribution of reactive groups. This random distribution of reactive groups would stabilize the nanostructure homogeneously, causing a cocontinuous dispersion of nanophase structure within the matrix.

PVDF is a technologically important polymer because of its piezo and pyroelectric properties.[18] Polythiophene and its derivatives are also important members of the conducting polymer family because of its excellent conducting, electroluminescence, and nonlinear optical properties.[19] Thus, the blends of nanostructure polythiophene derivative in the PVDF matrix may show interesting optoelectronic properties suitable for sensor and optoelectronic applications. There is a report of macro-phase-separated blend of trifluorethylene copolymer of PVDF and P3HT prepared by the interpenetrating network

---

* To whom correspondence should be addressed. E-mail: psuakn@mahendra.iacs.res.in.

Nanostructured PTMA within PVDF Matrix

J. Phys. Chem. B, Vol. 114, No. 7, 2010 **2343**

SCHEME 1: Schematic Phase Diagram of Nanostuctutred Polymer Blends Representing the Binodal and Spinodal Mode of Phase Separation
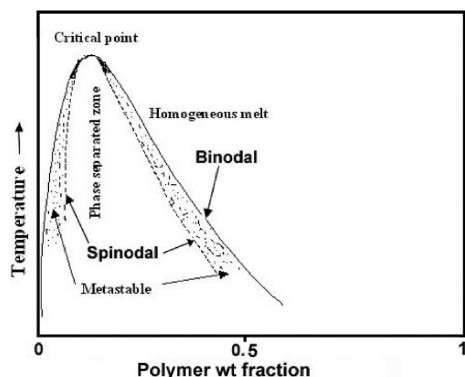
formation technique.[10] In the present PVDF−PTMA blend, we have used the reactive blending technique to obtain a cocontinuous distribution of PTMA nanostructure in the PVDF matrix. In the PTMA, the methyl acetate group has been introduced in the 3- position of the thiophene ring and polymerized. The $>C=O$ group of PTMA is expected to interact with the $>CF_2$ group of PVDF,[20–22] and if the PTMA can be made in nanodimension, cocontinuous nanostructured polymer blend would result.

The polymer blends may exhibit upper critical solution temperature (UCST) and lower critical solution temperature (LCST) depending on the nature of interaction between the components.[23,24] A strong specific interaction usually results in LCST, while a weak dispersive interaction results in an UCST type phase diagram. The nanostructured blends are prepared by cooling the mixtures from the melt state, and this blend is expected to show liquid−liquid phase separation of UCST type during cooling for weak dispersion interaction in this system because of strong affinity between own pair of contacts. The phase separation may take place by binodal or by spinodal decomposition (Scheme 1); the former occurs by a nucleation and growth process with downhill diffusion, while the latter occurs by spontaneous fluctuation with uphill diffusion.[25–27] If a system is near the critical composition, the system may undergo spinodal decomposition because it would not get enough time for the growth of phase separated nuclei due to the narrow metastable region. Thus, the size of phase separated domains may depend on the above phase separation mechanism and spinodal decomposition may result in interconnected smaller size nanophases. In this manuscript, the probable cause of formation of different size PTMA nanodomains within the PVDF matrix has been illuminated from the above immiscibility mechanisms in the melt state and an account of the variation of the physical and conducting properties of the nanoblends from those of the bulk polymers would be presented here. Also, any difference in the above physical and optoelectronic properties due to difference in nanophase separation mechanisms has been carefully established. To our knowledge, it is a first time report where both binodal and spinodal decompositions are identified from the shapes and sizes of PTMA nanodomains and also from the difference in optical and electronic properties of the PVDF−PTMA nanostructured blend.

Experimental Section

Samples. Poly(vinylidene fluoride) (PVDF) ($\bar{M}_w = 180\,000$, PDI = 2.57) was purchased from Aldrich Chemical Co. (USA).

The head to head (H−H) defect of the polymer is 4.33 mol %[28] as obtained from ^{19}F NMR spectra in DMF-d_7 solution.

Poly(3-thiophene methyl acetate) (PTMA) is synthesized by polymerizing 3-thiophene methyl acetate (TMA), prepared by refluxing 3-thiophene acetic acid (TAA, purchased from Aldrich Chemical Co., USA) in dry methanol with a drop of conc. H_2SO_4 as catalyst for 24 h. The protected monomer 3-thiophene methyl acetate (TMA) is polymerized by chemical oxidation coupling in dry $CHCl_3$ using anhydrous $FeCl_3$. The molar ratio of the oxidant to monomer is taken as 4:1. The mixture is stirred at 0 °C under N_2 for 24 h. The resultant mixture is poured into a large excess of methanol to precipitate PTMA. The crude polymer is washed with methanol and deionized water by Soxhlet extraction to remove residual oxidant and oligomers. The brown-red polymer is dissolved in $CHCl_3$ and is dried in a vacuum at 60 °C for 3 days.[29] The molecular weight of PTMA is measured by gel permeation chromatography (GPC, Waters) in THF solvent using Ultrastyragel column and polystyrene as standard at 30 °C. The weight average molecular weight ($\bar{M}_w$) of the polymer is 7.1×10^3, and the polydispersity index (PDI) is 2.74. The head−tail (H−T) regioregularity of the polymer is measured using ^1H NMR spectra in $CDCl_3$ (Supporting Information, Suppl. Figure 1). From the peak areas of the α-methylene peak at 1.61 (H−H) and 3.72 and 3.76 (H−T) ppm, the percentage of H−T regioregularity is calculated to be 66 mol %.[30]

Preparation of Nanostructure Blend. 4% (w/v) stock solutions of PVDF and PTMA are separately made in dry *N,N*-dimethyl formamide (DMF). They are mixed in different proportions to obtain different weight percents of PTMA (1, 3, 5, 15, and 25) with respect to PVDF weight in the blend. The samples are designated as PTMA1, PTMA3, etc., where the number indicates the percentages (w/w) of PTMA in the blends. The mixed solutions are stirred well using a magnetic stirrer at 40 °C. The solutions are evaporated on flat dishes at 50 °C and are finally kept in a vacuum at 60 °C for 3 days. The sample films have color from yellow to red depending on the concentration of PTMA. The samples are then melted at 230 °C for 5 min and are cooled to 30 °C by switching off the Mettler (FP-82) hot stage to get the nanoblend.

Microscopy. The TEM morphologies of the films are studied using the above melt-cooled films and taking a thin section of the film (~70 nm thickness) at −80 °C with a cryo-microtome (Ultracut R Leica) using diamond knife. The TEM images are taken by placing the above thin sections on a carbon coated copper grid and observing through a JEOL high resolution transmission electron microscope (model 2010EX) operated at an accelerated voltage of 200 kV without staining. A CCD camera was used to take the picture. The optical microscopy of the isothermally crystallized sample ($T_c = 140$ °C) is done using a Leitz Biomed Optical Microscope with a perfectly crossed polarizer. The pictures are taken in a Leitz digital camera. The isothermal crystallization is made in a Mettler FP-82 hot stage after melting the sample film (~20 μm thickness) at 230 °C and then quenching to 140 °C at the hot stage for 3 h.

Thermal Property. The differential scanning calorimetry (DSC) of the blend samples are made in a Perkin-Elmer Differential Scanning Calorimeter (Diamond DSC-7) with Pyris Software. The instrument is calibrated with indium before each set of experiments. The samples (3−4 mg) are taken in aluminum capsules, crimped, and heated from 40 to 230 °C at the heating rate 40 °C/min under a nitrogen atmosphere. The higher heating rate was chosen to avoid the melt recrystallization.[31,32] The sample is then kept at 230 °C for 5 min and cooled at the

2344 *J. Phys. Chem. B, Vol. 114, No. 7, 2010*

Manna et al.

cooling rate 5 °C/min to 40 °C where it is kept for 10 min for crystallization. Then, the samples are again heated to 230 °C at the heating rate 40 °C/min. The heating and crystallization temperatures are taken as the peak temperature, and the enthalpy values are obtained from the peak area using the Pyris software of the computer.

The thermogravimetric analysis (TGA) experiments are performed using a TA Instruments (model SDT Q 600) under a nitrogen atmosphere at a heating rate of 10 °C/min.

X-ray Scattering. The wide-angle X-ray scattering (WAXS) experiments are performed on the melt-cooled films. The experiment is carried out in a Bruker AXS diffractomer (model D8 Advance) using a Lynx Eye detector. The instrument was operated at a 40 kV voltage and at a 40 mA current. The sample is scanned in the range $2\theta = 5-45°$ at the scan rate 0.5 s/step with a step width of 0.02°.

For small angle X-ray scattering (SAXS) measurement, a scintillation counter detector is used with a scan rate of 1 s/step with a step width of 0.02°. The samples are scanned in the 2θ range 0.1−5°, and the data were Lorentz corrected.

Spectral Measurement. The UV−vis spectra of the melt-cooled films (2−4 μm thickness) of the nanoblends are performed using a UV−vis spectrophotometer (Hewlett-Packard model 8453) at 30 °C. A blank run of an empty cover-slip is taken first, and the blank spectrum is subtracted from the sample spectra in each case.

The photoluminescence (PL) spectra of the above melt-cooled films are performed in a Fluoromax-3 instrument (Horiva Jovin Yvon). The photoexcitation is made at a 75° angle using 370 nm radiation, and the emission is detected at a right angle with respect to the excitation beam direction. Each spectrum is normalized with a film thickness of 1 μm for comparison; the film thickness is measured using a Profilometer.

The FTIR spectra of the samples are obtained from the films in a Shimadzu FTIR (model-8400S) instrument.

Mechanical-Property Measurement. The dynamical mechanical property of the sample is measured using a Dynamic Mechanical Analyzer (DMA) (TA Instruments, model Q-800). Films of a particular dimension (25 mm × 5 mm × 0.15 mm) are made by solution casting on a die and then melt-cooled at the Mettler Hot Stage. The samples are heated from −100 to 150 °C in the DMA at a heating rate of 10 °C/min. The storage modulus (G'), loss modulus (G''), and tan δ are measured at a constant frequency of 1 Hz with a static force of 0.02 N.

dc Conductivity Measurement. The dc conductivity of the sample is measured by a two-probe method using an electrometer (Keithley model - 617). The thin film (thickness ∼0.01 mm) of the sample is made by melting the sample at 230 °C at the Mettler hot stage and gently pressing by a thick glass slab. The thickness of the film is measured by using screw gauze, and the film is then gold coated by the vacuum deposition technique. This film is then connected to the electrometer through a copper wire using silver paste. The resistance is measured, and the conductivity (σ) is calculated from the equation

$$\sigma = \frac{1}{R} \times \frac{l}{A}$$

where "l" is the thickness and "A" is the area of the films; the latter is measured from the gold-coated area by measuring the diameter using slide calipers.

For conductivity measurement at different temperatures, the gold coated sample is placed on a brass platform separating from it by a mica plate. A low-voltage heater and a thermo-couple are inserted into the platform. Heater temperature is controlled using a SELEC PID500 controller and a dimerstat. The sample holder is covered with a glass jar to avoid draft. The temperature was raised from 30 to 130 °C at an interval of 5 °C. After waiting for 2 min at each temperature for thermal equilibrium, the resistance of the sample is measured with a Keithley electrometer (model 617) using the two-probe technique. The current−voltage (I−V) characteristics of the films (thickness ∼0.01 mm) are studied by using the same sample from −5 to +5 V, and the current is measured at each applied voltage. The voltage is varied by an increment rate of 0.05 V in 13 s.

Result and Discussion

Morphology. In Figure 1a and in Suppl. Figure 2 in the Supporting Information, the TEM micrographs of the PVDF−PTMA hybrids are presented. From the figures, it is apparent that there are dark spherical spheres dispersed in the gray PVDF matrix. The dark phase may be attributed to PTMA because of its high electron density due to the presence of conjugated π bonds in the polymer. The nanophases are almost spherical in nature, and its size shows a minimum with 5% (w/w) PTMA concentration and becomes agglomerated at ≥25% (w/w) PTMA concentration (Supporting Information, Suppl. Figure 2). The sizes of the nanophases are 49 ± 9, 56 ± 8, 4.4 ± 0.6, 18 ± 3, and 37 ± 4 nm for PTMA1, PTMA3, PTMA5, PTMA15, and PTMA25, respectively, and the plot of the nanophase sizes with composition (Figure 1d) clearly present a minimum for ∼5% PTMA concentration. Further, the PTMA nanophases in PTMA5 are somewhat overlapped that appears to be interconnected which may be confirmed later from photoluminescence and I−V property measurements.

This is an interesting observation, and no definite reason is known. One probable explanation may lie in the difference of phase separation mechanism from the homogeneous melt, e.g., binodal or spinodal decomposition during the binodal decomposition, the phase separation occurs at equilibrium condition, i.e., the chemical potential of a component in one phase is equal to that in the other phase. Under such equilibrium conditions, the phase separation occurs by a nucleation and growth mechanism[25–27,33,34] causing larger size particles. Probably for PTMA5, the system quickly crosses the binodal and spinodal regions because of the sharp convex downward nature of the temperature vs composition plot (dark shaded area, Scheme 1, also see phase diagram in the DSC section) and the 5% (w /w) PTMA concentration is probably close to the critical composition. As the gap between the binodal and spinodal is narrow, there may be no nucleation and growth; rather, phase separation occurs by spontaneous fluctuation and uphill diffusion as proposed by Cahn and Hilliard causing spinodal decomposition.[25–27] Under this situation, the phase domains are smaller than those in the nucleation and growth process, as there is no time of growth of the nuclei and the separated phase have very high interconnectivity. This matrix polymer then crystallizes on cooling, stabilizing the PTMA nanophase which also solidifies in the cooling process. Thus, it may be argued that at PTMA5 the smaller size nanophase is due to the spinodal decomposition. However, certainly a question may arise as to why the nanophase is smaller in size only for the PTMA5 sample. A calculation of spinodal curve is made taking an approximation of critical temperature to be 200 °C for the system, and it is presented in the phase diagram (cf. DSC section) showing critical composition at ∼6 wt % PTMA in the nanoblend (Supporting Information). In Suppl. Figure 2c in the Supporting Information, the
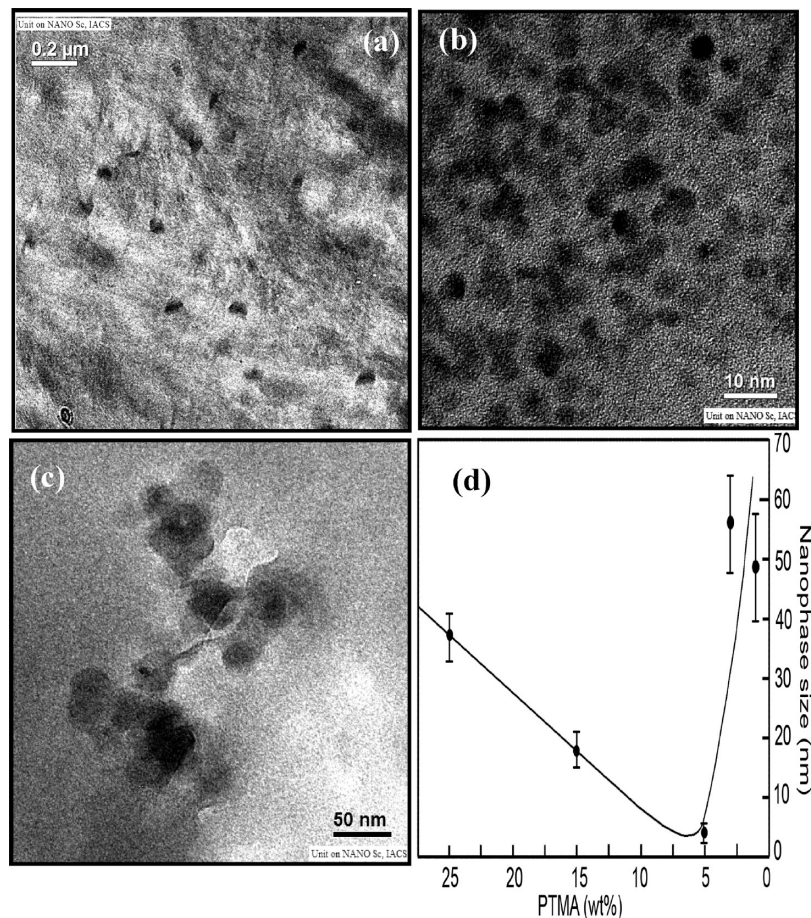
Figure 1. Transmission electron micrographs (TEM) of PVDF−PTMA nanoblends: (a) PTMA3; (b) PTMA5; (c) PTMA25. (d) Nanophase size vs PTMA concentration (wt %) curve.

EDXS spectrum of the marked portion of Suppl. Figure 2b indicates the presence of both sulfur and fluorine; probably the fluorine is coming from the diffuse interfaces of PTMA nanoparticles characterizing cocontinuous structure of the nanoblends.

The polarized optical micrographs of the nanoblends are presented in Figure 2 for isothermally crystallized samples at 140 °C. It is apparent from the figure that pure PVDF has compact spherulitic structure, but for PTMA5, the PVDF spherulites are disorganized and the four lobes of the spherulites are totally absent. Again, the PTMA domains are seen as interconnected small brown spots supporting the spinodal decomposition in the PTMA5 sample. However, in PTMA25, the red spots of PTMA are very large and are not interconnected with each other, probably as a result of binodal decomposition. The phase structures of PTMA in the optical micrographs are much larger in size than that observed in TEM pictures (Figure 1). One probable reason is the nanophase PTMA that comes out from the bulk to the surface can agglomerate easily for the lesser diffusion barrier than that in the bulk having a highly viscous PVDF matrix. Also, the thickness of the films used for optical microscopy is ∼20 μm which is 667 times greater than the diameter of individual PTMA spheres (∼30 nm from TEM). Thus, many such spheres are encountered in the light path through the films showing a larger size of PTMA nanparticles in the optical microscopy.

X-ray Diffraction. The WAXS diffraction patterns of the PVDF−PTMA nanoblends are presented in Figure 3. From the figure, it is evident that PVDF has peaks at $2\theta = 17.8, 18.40, 20.1$, and $26.8°$ which correspond to the α-polymorph of PVDF
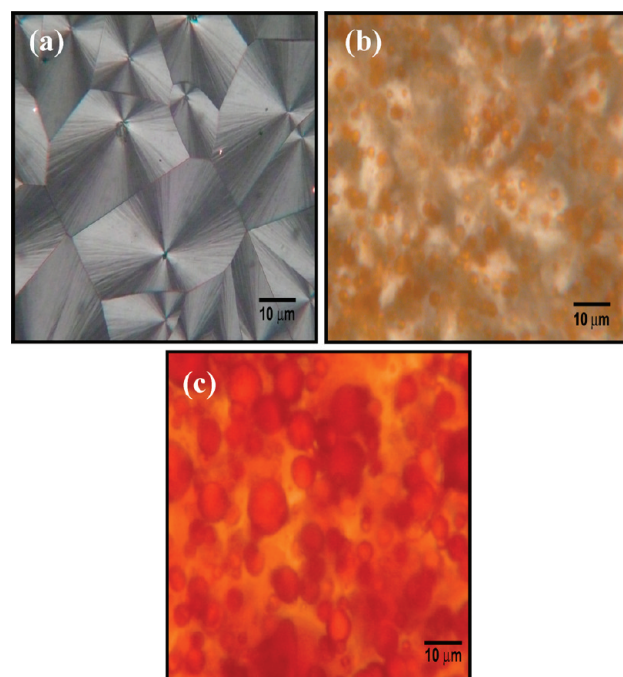

Figure 2. Polarized optical micrographs of PVDF−PTMA nanoblend systems (a) PVDF, (b) PTMA5, and (c) PTMA25 produced by isothermal crystallization ($T_C = 140 °C$) on a glass slide under a N_2 atmosphere.

in the hybrid.[35–38] On addition of PTMA, the α-peak of PVDF is retained, indicating no change in the crystal structure due to

2346 *J. Phys. Chem. B, Vol. 114, No. 7, 2010*

Manna et al.
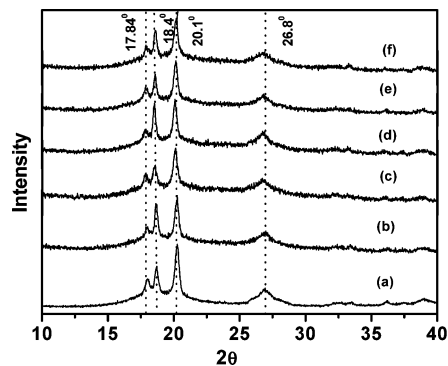
Figure 3. WAXS patterns of neat PVDF and PVDF−PTMA blends: (a) PVDF; (b) PTMA1; (c) PTMA3; (d) PTMA5; (e) PTMA15; (f) PTMA25. The number indicates the weight percentage of PTMA in the blends.
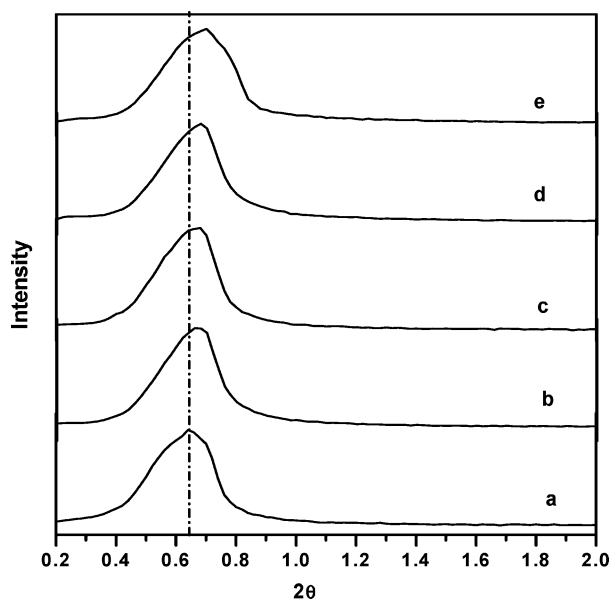
Figure 4. Lorentz-corrected SAXS pattern of neat PVDF and PVDF−PTMA nanoblends: (a) PVDF; (b) PTMA3; (c) PTMA5; (d) PTMA15; (e) PTMA25.

TABLE 1: Variation of Different Crystalline Thicknesses of PVDF in the Nanoblends

	long distance (nm)	crystallinity[a]	lamellar thickness (nm)	amorphous overlayer thickness (nm)
PVDF	13.8	0.46	6.35	7.45
PTMA3	13.3	0.45	5.98	7.32
PTMA5	13.1	0.45	5.90	7.20
PTMA15	12.9	0.46	5.93	6.97
PTMA25	12.5	0.47	5.87	6.63

a Normalized to the PVDF concentration in each blend.

blending. PTMA is an amorphous polymer,[29] and also, it is immiscible in the polymer blend. Thus, the WAXS patterns of the α-phase remain unchanged for the nanostructure PTMA in the matrix.

In Figure 4, the Lorentz-corrected SAXS patterns of the nanoblends are presented. It is apparent from the figure that there is a shift of the SAXS peak to the higher 2θ value with an increase of PTMA concentration, resulting in a decrease of long period (Table 1). The decrease in long period of PVDF may arise from the change of amorphous overlayer and lamellar thickness of PVDF crystal by the attractive force of PTMA
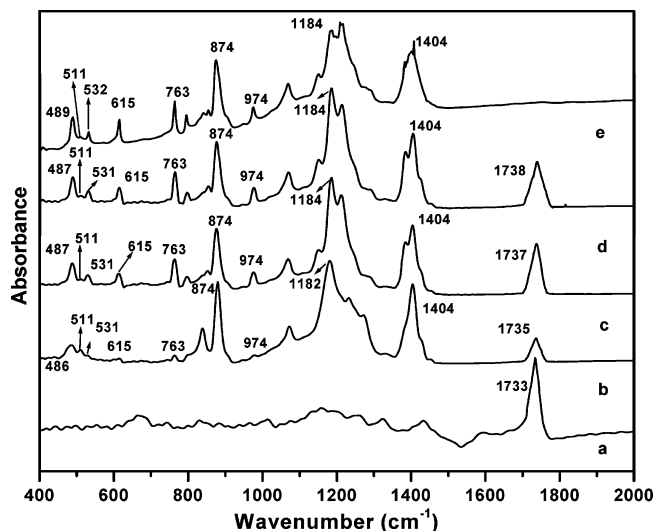

Figure 5. FTIR spectra of neat PVDF and PVDF−PTMA blends: (a) PTMA; (b) PTMA3; (c) PTMA5; (d) PTMA15; (e) PVDF.

nanodomains due to its large surface area. The inherent assumption in analyzing the SAXS data is that form factor scattering (scattering due to individual particle shape and size) is not affecting where the maximum appears.

FTIR Spectra. From the FTIR spectra of PTMA and the nanoblends (Figure 5 and Suppl. Figure 3 in the Supporting Information), it is apparent that the $>C=O$ peak of PTMA shifts to the higher energy from 1733 to 1738 cm^{-1} due to the nanophase formation with an exception to PTMA25 where the peak is at the same frequency as in pure PTMA. Also, in all of the spectra of the blends, there is no shift of the PVDF peaks, indicating the absence of any interaction between PVDF and PTMA. It is to be noted here that in the entire blend spectra there are peaks at 794, 615, and 531 cm^{-1} characterizing the formation of the α-polymorph of PVDF.[39,40] The specific interaction between the components is usually evident from the $>C=O$ peak position shift to lower energy, but here a shift to higher energy occurs, showing the higher bond order of the $>C=O$ linkage. These indicate that the $>C=O$ group is not fully polarized and it may be attributed to the π clouds of the whole chain of conducting polymer. These π clouds being negatively charged have a tendency to repel the loan pairs of electrons of oxygen and pushes them somewhat toward the $\overleftarrow{C=O}$ direction, inhibiting its full polarization as $>C^{\delta+}-O^{\delta-}$. This reduces the interaction of the $>C=O$ group with the $>CF_2$ dipole of PVDF, causing immiscibility of the PTMA−PVDF system. The extent of immiscibility is however lower than that in the macro-phase-separated P3HT−PVDF−TrFE system[10] because of the presence of the $>C=O$ polar group. Thus, it may be surmised that due to the lesser extent of interaction between PTMA and PVDF than that in acrylate/vinyl acetate with PVDF,[21,22] nanophase separation takes place.

Differential Scanning Calorimetry. The heating and cooling thermograms of the nanostructured PTMA−PVDF blends are presented in Figure 6A and B and Suppl. Figure 4 in the Supporting Information. In Figure 6A, there is a single melting peak in all of the blends, and the melting point has increased by 2−3 °C for PTMA1, PTMA3, PTMA5, and PTMA15. However, in PTMA25, the melting point remains the same as in pure PVDF. From SAXS results (Table 1), it is evident there is a decrease of lamella thickness in the nanoblends. Usually with a decrease of lamella thickness, the melting point of polymer crystal decreases. However, when there are nanophases

Nanostructured PTMA within PVDF Matrix

J. Phys. Chem. B, Vol. 114, No. 7, 2010 **2347**

(A)

(B)

(C)
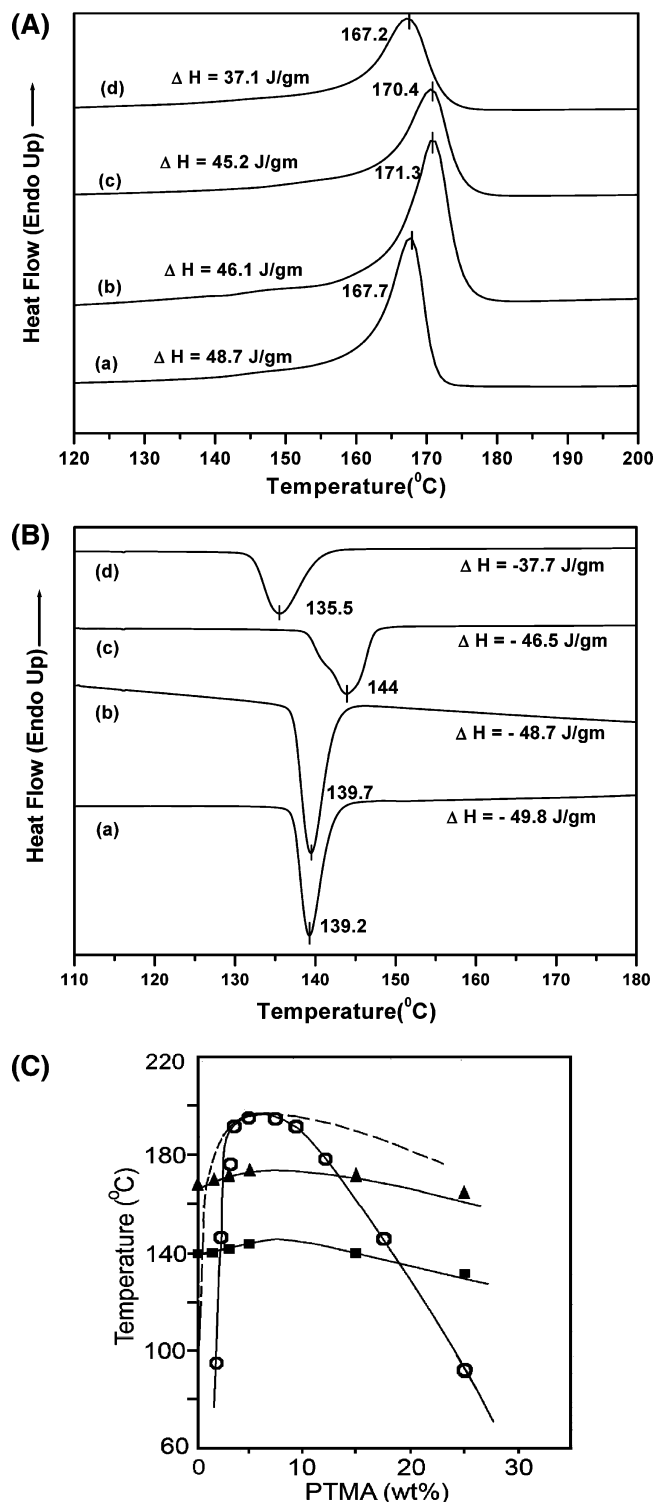
Figure 6. (A) DSC thermograms for neat PVDF and PVDF−PTMA blends during heating at the scan rate 40 °C/min: (a) PVDF; (b) PTMA3; (c) PTMA5: (d) PTMA25. (B) DSC thermograms for neat PVDF and PVDF−PTMA blends during cooling from the heterogeneous melt at 5 °C/min for (a) PVDF, (b) PTMA3, (c) PTMA5, and (d) PTMA25. (C) Phase diagram of the PVDF−PTMA blend system. The symbol ▲ denotes the melting peak temperature, the symbol ■ denotes the crystallization peak temperature, the symbol O denotes calculated spinodal points, and the dashed curve denotes the anticipated binodal.

within the composite, a different phenomenon may happen because of the large surface forces of the nanophases. This confined crystal within the nanophases requires a higher energy

to melt the crystal.[41,42] Also, the nanophases sometimes act as a thermal barrier and hence required a higher temperature for melting (cf. the TGA section). In Figure 6B and in Suppl. Figure 4b in the Supporting Information, the crystallization isotherms are shown for the PTMA nanoblend and here also the crystallization temperature shows a maximum for PTMA5. The reason for the highest crystallization temperature for PTMA5 might be attributed to the liquid−liquid phase separation, and the nature of the phase diagram shown in Figure 6C is similar to that type.[34,43] The number density of phase-separated domains is very large with the lowest size at this composition because of spinodal decomposition. Thus, a large surface is available for surface nucleation of PVDF,[44] showing higher crystallization temperature due to phase mixing. In Figure 6C, the calculated spinodal (see the Supporting Information) and an anticipated binodal of the system are presented. It is apparent from the figure that the system phase separates after melting and becomes homogeneous above the binodal. Thus, on cooling the melt from 230 °C, PTMA5 immediately crosses the binodal and spinodal boundaries and phase separation occurs by spinodal decomposition. However, this is not the case for the other compositions where the phase separation may occur by nucleation and growth processes because of a large gap between the boundaries of binodal and spinodal curves. A distinction between binodal and spinodal decompositions of different blends may be evidenced from the difference in optical and electronic behavior discussed in the following sections. The apparent enthalpy of fusion/crystallization decreases with an increase of PTMA concentration, but the normalized enthalpy values do not change, indicating the crystallinity of PVDF remained unchanged in the nanoblends (Table 1).

Polymer crystals have the switchboard model structure consisting of crystalline lamella, amorphous overlayer, and interface between the two.[45] The crystallinity, long distance, lamella thickness, and amorphous overlayer thickness values are presented in Table 1. The lamella thickness has been obtained by multiplying SAXS long distance data with normalized crystallinity, and amorphous thickness has been obtained by subtracting the lamella distance from the long distance. It is apparent from the table that the amorphous overlayer thickness decreases by 11%, the lamella thickness decreases by 7.5%, and the long distance decrease by 10% from that of the pure component. The decrease of long distance is therefore due to the decrease of both amorphous overlayer thickness and the lamella thickness. The decrease of amorphous overlayer thickness may be attributed to the attractive force between the nanostructured PTMA compressing the amorphous overlayer of PVDF crystal. However, the decrease of lamella thickness is unexpected and perhaps it reflects the decrease of interface thickness between the crystalline lamella and amorphous overlayer thickness. This assertion might be true because this decrease is much less than that of the amorphous layer, signifying that the lamella−amorphous interface is not sharp but diffuse in nature. Both the reduced interface and the reduced amorphous overlayer thickness may cause a small increase in the melting point of crystal lamella because it needs additional energy to release the tighter boundaries to begin the motions of the motifs present in the lattice and hence to start melting of the crystal.

Thermogravimetric Analysis. In Figure 7 and Suppl. Figure 5 of the Supporting Information, the TGA thermograms of PTMA blends are presented. It is evident from the figure that the degradation temperatures of the nanoblends have increased significantly. The degradation temperatures calculated
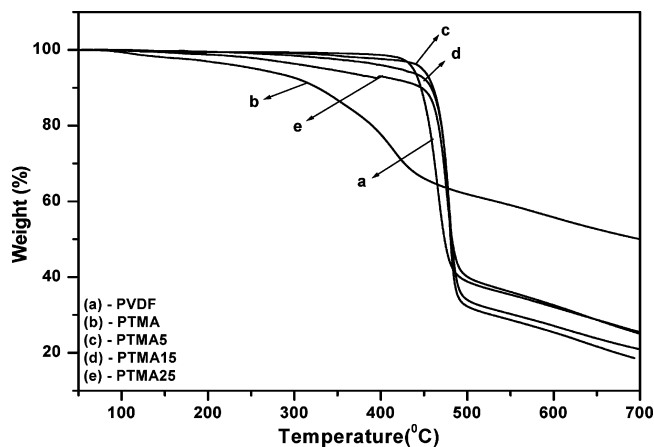
Figure 7. TGA thermograms of neat PVDF and PVDF−PTMA nanoblends in the presence of N_2 gas with a heating rate of 10 °C/min.
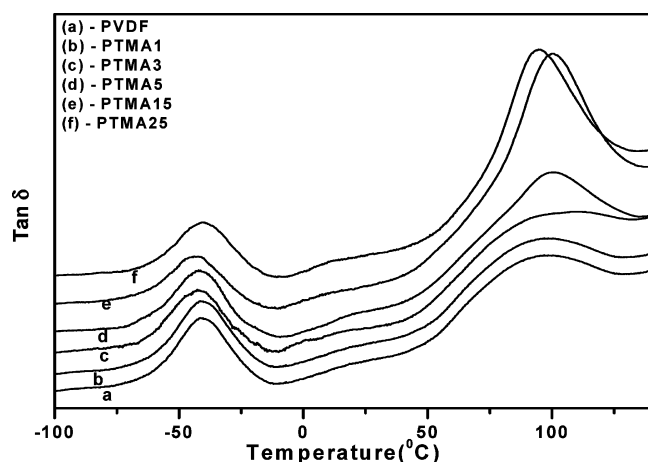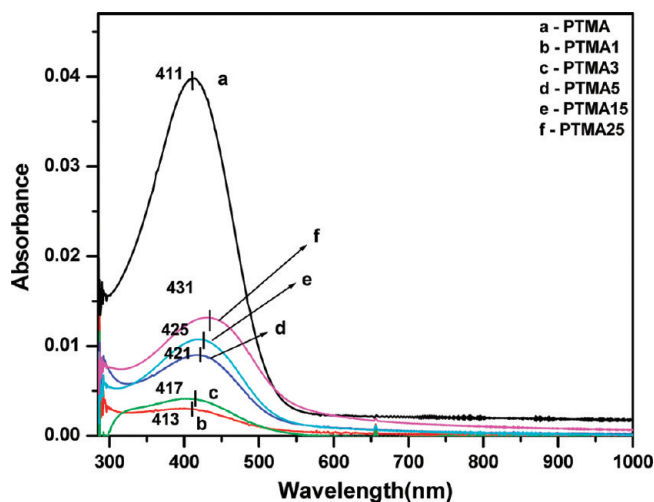

Figure 8. Tan(δ) as a function of temperature for PVDF−PTMA blends: (a) neat PVDF; (b) PTMA1; (c) PTMA3; (d) PTMA5; (e) PTMA15; (f) PTMA25.
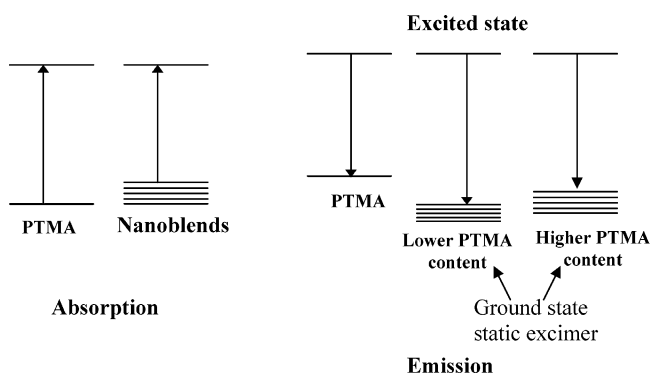

Figure 9. UV−vis absorption spectra of PVDF−PTMA blend films in the melt-cooled state (normalized to 1 μm film thickness).

from the intersection of the tangents of the horizontal and vertical lines of the thermograms are 447, 469, 464, 470, 467, 463, and 355 °C for PVDF, PTMA1, PTMA3, PTMA5, PTMA15, PTMA25, and PTMA samples, respectively.

The increase in degradation temperature of PVDF may be explained from the PTMA nanostructure that acts as a heat barrier due to the large surface area of PTMA nanophase hindering the degradation process. It is also important to note that the residual weight increases with an increase in PTMA concentration in the nanoblend. The PTMA has also very high residual weight, probably due to the aromatic thiophene ring which is stabler than that of PVDF for its resonating structure. The PTMA5 showed higher degradation temperature than that of others because of the higher density of PTMA nanophases yielding a more effective barrier for diffusive processes.

Dynamic Mechanical Analysis (DMA). In Figure 8, the tan δ vs temperature plots of PTMA blends are presented. The lower temperature peak at −40 °C corresponds to the glass transition temperature of the PVDF.

From the tan δ plot, it is evident that the glass transition temperature of PVDF is invariant for the different blend compositions. This invariant glass transition temperature suggests that PVDF−PTMA blends are immiscible,[23,24] showing nanophase separation in the melt of the blend. It is to be noted here that there is another prominent peak at higher temperature (∼100 °C) in PVDF and also in the blend. This peak corre-

sponds to the relaxation of the interface between the crystalline and amorphous region.[7,46] In the blends, there is a 4−5 °C increase in this relaxation temperature, indicating the interface is compact in the blend. This is also supported from the SAXS and DSC data which indicate a reduced interfacial thickness in the nanoblends. In PTMA25, this temperature remains almost unchanged as in pure PTMA similar to that in melting point and >C=O vibration peak characterizing this system to behave like a macro-phase-separated system. It is also of interest to discuss the unchanged T_g data of PVDF (cf. the DMA section) in spite of the reduced long distance (cf. SAXS result), indicating a more compact PVDF in the nanoblend than that in pure PVDF. Usually a more compact matrix structure causes a small increase of T_g because of the difficulty of relaxation,[42] but here, the invariant T_g means that the T_g change is too small or the change is compensated by some other factors. As the nanophase of PTMA has a large interface, partial mixing of PVDF chains at the interface might occur for the weak dipolar interaction, causing some decrease of T_g and compensating the T_g increase due to compactness. It is to be noted that the storage modulus of the nanoblends does not increase in the nanoblends; rather, there is a small decrease in the storage modulus (Supporting Information, Suppl. Figure 6) which is contradictory to that usually observed in polymer composites.[42] No definite reason for the decrease of storage modulus can be afforded here. Probably, PTMA has a small molecular weight (degree of polymerization = 17) and the amorphous PTMA behaves almost as a liquid-like system. Consequently, the reinforcement effect of nanostructured PTMA on the PVDF matrix is negligible.

UV−vis Spectroscopy. The UV−vis spectra of the melt-cooled films of nanostructured PTMA blends are presented in Figure 9. From the figure, it is apparent that the $\pi−\pi^*$ transition band of PTMA becomes red-shifted and the absorption intensity becomes reduced with increasing PTMA concentration in the nanostructured blends. There are two main reasons for the red shift: (i) increase of the conjugation length due to interaction with PVDF for blending and (ii) aggregation of the PTMA chain[47] causing delocalization of π electrons by $\pi−\pi$ interaction. The first reason may not be acceptable here because of nanophase separation of PTMA and PVDF in the blend, indicating the absence of intermolecular interaction. Thus, it might be possible that the PTMA chain becomes aggregated. Here, the aggregation is of intramolecular (i.e., intrachain) type. Due to $\pi−\pi$ interaction of the thiophene rings in the isolated

SCHEME 2: Representative Energy Diagram of PVDF−PTMA Nanoblends Explaining the Red Shift and Blue Shift in the Absorption and Emission Spectra, Respectively

Figure 11. dc conductivity vs temperature plots of PTMA and PVDF−PTMA nanostructured blends at indicated composition.

PTMA chains of the nanophase, the chain segments become aggregated and may cause a decrease of root-mean-square end-to-end distance. Such an intrachain aggregation of segments of PTMA molecules causes delocalization of π orbitals and hence a decrease of the band gap, showing a red shift (Scheme 2). The decrease of normalized intensity is due to the decrease of PTMA concentration in the nanoblends; the lower the PTMA concentration, the lower is the absorbance value.

Photoluminescence Spectra. In Figure 10, the normalized PL spectra of PTMA and its blends are presented. It is apparent from the figure that in the nanoblend there is a blue shift of the emission peak and it decreases gradually with an increase in PTMA concentration. A probable reason for the blue shift is due to the nanostructure PTMA formation when the individual PTMA chain becomes aggregated. After reaching the excited state, the PTMA molecules emit energy passing through a conformational change and promoting more effective aggregation. This aggregation causes lowering of the ground state energy which may be termed as "static excimer" formation, and this higher aggregated ground state has lower energy than that of the original ground state, causing a blue shift. Similar static excimer formation with the lower energy ground state is possible as observed in static pyrene excimers with calixerene and binapthyl crown ether systems.[48,49] At lower PTMA concentration, PVDF helps to stabilize the PTMA nanophase more than that at higher PTMA concentration by preventing aggregation between nanophases. As a result, the intramolecular aggregation of PTMA chains is higher, causing the highest blue shift in the
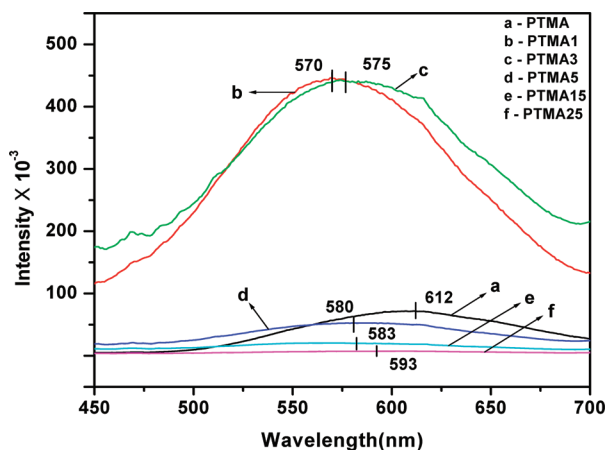
Figure 10. Photoluminescence (PL) spectra of PVDF−PTMA blend films at melt-cooled state (normalized to 1 μm film thickness).
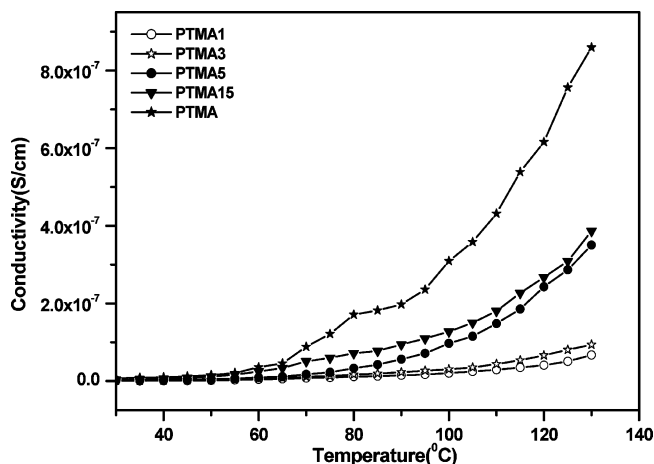
lower PTMA concentration in the blend. The normalized spectra exhibit dramatically higher intensity for the nanoblends than that of the pure PTMA at the lower concentration region. The PTMA1 and PTMA3 show ∼8 times higher PL intensity than that of the pure PTMA. The reason for the sharp increase of PL intensity of PTMA1 and PTMA3 is due to the nanostructure where quenching with other PTMA chains is lesser than that in the bulk. Also, the distance between the PTMA spheres is large, preventing quenching between neighboring PTMA spheres. In PTMA5, there is interconnectivity between the nanodomains (due to spinodal decomposition), so nonradiative decay is almost the same as that in pure PTMA, showing similar PL intensity as in the bulk. With PTMA15 and PTMA25, the nanophases are produced in a very large amount and they are also large in size in the later case. Thus, quenching can occur between the neighboring PTMA spheres as the distance between them is lower, causing the decay of excitons similar to that in the bulk PTMA.

dc Conductivity. The dc conductivity values of the PTMA nanoblends in the undoped state at 30 °C are 7.1, 0.6, 1.2, 2.5, 2.4, and 2.5 nS/cm for the PTMA, PTMA1, PTMA3, PTMA5, PTMA15, and PTMA25 samples, respectively. Thus, there is a decrease of conductivity in the nanoblend as compared with the pure PTMA. The UV−vis spectra showed a red shift of the $\pi-\pi^*$ transition band; hence, an increase of conductivity should occur. However, the opposite result supports our previous argument that the red shift is not due to the increase of conjugation length. Thus, the red shift of the $\pi-\pi^*$ transition band is definitely due to the intramolecular aggregation of PTMA segments in the chains. This aggregation of PTMA chain causes intrachain twisting, yielding a lower conductivity in the nanoblend than that of pure PTMA. The lowest composition of the blend studied here is crossing the percolation threshold as PTMA1 has a good value of conductivity which is 1 order lower than that of pure PTMA but has almost the same value as that of the other nanoblends.

Also, there is an increase of conductivity with the PTMA content in the nanostructured blends. Probably due to the increase of nanophase density and the interconnected nature of the PTMA domains, the conductivity is gradually increasing in the nanoblends.

In Figure 11, the conductivity data measured at different temperatures (30−130 °C) are presented. It is evident from the figure that with an increase in temperature conductivity increases in every case, indicating the semiconducting nature of the blends. The PTMA, PTMA5, and PTMA15 show a much higher

2350 *J. Phys. Chem. B, Vol. 114, No. 7, 2010*

Manna et al.
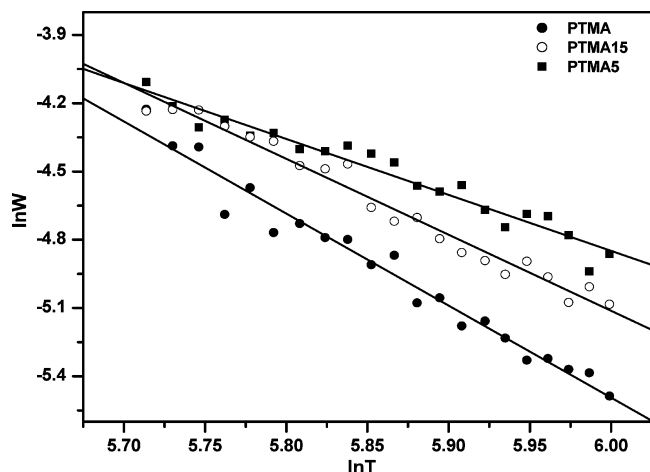
Figure 12. ln *W* vs ln *T* plots for pure PTMA, PTMA5, and PTMA15 blends.

increase in conductivity with temperature than that of the others. In the log σ vs 1000/*T* plot (Supporting Information, Suppl. Figure 7), there is a hump at ~65 °C for each sample, indicating the presence of a transition temperature. In analogy with P3HT and its cocrystals,[50] it may be argued that a conformational transition of PTMA chain may occur at this temperature. To understand the conduction mechanism fully, we have analyzed the data according to the equation representing the one-dimensional variable range hopping model as transport properties of conducting polymers are commonly one-dimensional:[51]

$$\sigma = \sigma_0 \exp - (T_0/T)^{1/2} \qquad (1)$$

where σ is the conductivity at a particular temperature (*T*), σ_0 is the pre-exponential factor, and T_0 is a characteristic temperature. The logarithmic variation of eq 1 can be expressed as

$$\ln W = \ln 1/2 + 1/2 \ln T_0 - 1/2 \ln T \qquad (2)$$

where $W = \delta \ln \sigma / \delta \ln T$. Thus, a plot of ln *W* vs ln *T* should yield a straight line with a negative slope of 0.5. The ln *W* vs ln *T* plots are shown in Figure 12 and in Suppl. Figure 8 of the Supporting Information, where the slopes are negative in all cases and the values (4.0, 1.5, 1.7, 2.5, and 3.3 for PTMA, PTMA1, PTMA3, PTMA5, and PTMA15, respectively) are much higher than 0.5 of the one-dimensional variable range hopping model.

In analogy with P3HT and its blends, the higher slope may be explained from the conformational transition of the PTMA chain.[50] The conformational transition of the PTMA chain produces a larger number and better organization of conducting islands and hence a better charge hopping in the composite.

The decrease of conductivity in the nanoblends as compared with that of pure PTMA in spite of the red shift of the $\pi-\pi^*$ transition band in UV−vis spectra may be explained from the intramolecular aggregations of PTMA segments in the PTMA chain by the π stacking process. During this intramolecular aggregation, twisting of the PTMA chain occurs, decreasing the conjugation length and hence decreasing the conductivity. As the temperature increases, this conformational transition of PTMA chain may increase the conjugation length and it may also create a larger number and better development of conducting islands.[50] The processes are responsible for increasing the

charge hopping, causing the slope value to be larger than that of the one-dimensional variable range hopping model.

I−V **Characteristics.** The *I−V* characteristic curves of PTMA and its nanoblends are presented in Figure 13 and Suppl. Figure 9 of the Supporting Information. It is evident from Figure 13a that pure PTMA is a good semiconductor, but in nanoblends, some different behavior is observed. PTMA1, PTMA3, and PTMA15 show a negative hysteresis, but PTMA5 shows a memory effect. It may be argued that during the nanoblend formation some dipoles of PVDF get aligned at the interface of the PTMA nanophase and PVDF. These dipolar charges add to the current in the forward bias, but in the backward bias they put some hindrance on the current flow, resulting in negative hysteresis.[52] On the other hand, in PTMA5, there is some difference from that of other nanoblends, showing a memory effect. The inflection voltages are 4.15 and −4.15 V for the forward and backward bias, and the threshold voltages are 1.25 and −1.25 V. The difference in behavior might be due to the interconnected nature of the segregated phase of PTMA5 due to the spinodal decomposition. At the applied voltage of 4.1 V, the charge carrier reaches to the conduction band but it does not come back to the original position in the reverse bias at that voltage. Instead, the charge carrier becomes stabilized through the interconnected network until the voltage is dramatically reduced to 1.25 V, the threshold voltage. Thus, an electrical bistability appears in the PTMA5 nanoblend, causing a memory effect. This electrical bistability is not observed in other PTMA nanoblends, and this result supports the different nature of the phase separation (spinodal and binodal) in the nanoblends. This type of memory effect has been observed earlier in other nanocomposites, e.g., PVDF−multiwall carbon nanotube (MWNT) and poly(*o*-methoxy aniline)−Ag nanocomposites, where it is very much dependent on nanoparticle concentration and nanoparticle size.[52,53] At the present case, the memory effect is specific to the spinodal decomposition only where there is interconnectivity between the conducting phases. As the nanophase of PTMA has a large interface, partial mixing of PVDF chains at the interface might occur for a weak dipolar interaction. Such a situation is responsible for the partial alignment of the >CF_2 dipole toward the nanophase surface, and probably it adds to the current flow in the forward bias during *I−V* measurement. This small amount of interaction between PVDF and PTMA is responsible for the cocontinuous phase structure of PTMA nanophases in the PVDF matrix, facilitating effective charge transfer in the blends. Thus, due to the PTMA nanostructure formation in the blend, only a gradual red shift from the intrachain aggregation is occurring in the UV−vis spectra. However, remarkable changes are observed in PL and conductivity data, because of the occurrence of connectivity for exciton decay and for charge hopping in the nanostructured blends.

Conclusion

A successful preparation of PTMA nanostructure within the PVDF matrix is achieved by the reactive blending technique. The nanoparticle size at first decreases with an increase in PTMA concentration, showing a minimum for PTMA5, and then increases and becomes agglomerated at about 25% (w/w) PTMA concentration. Binodal and spinodal decomposition mechanisms of phase separation are used to explain the above variation of nanoparticle size, and spinodal decomposition could be a general procedure for obtaining very small size nanophases in the blends. To achieve spinodal decomposition, the composition of the blend should be chosen very close to the critical composition of the

Nanostructured PTMA within PVDF Matrix

J. Phys. Chem. B, Vol. 114, No. 7, 2010 **2351**
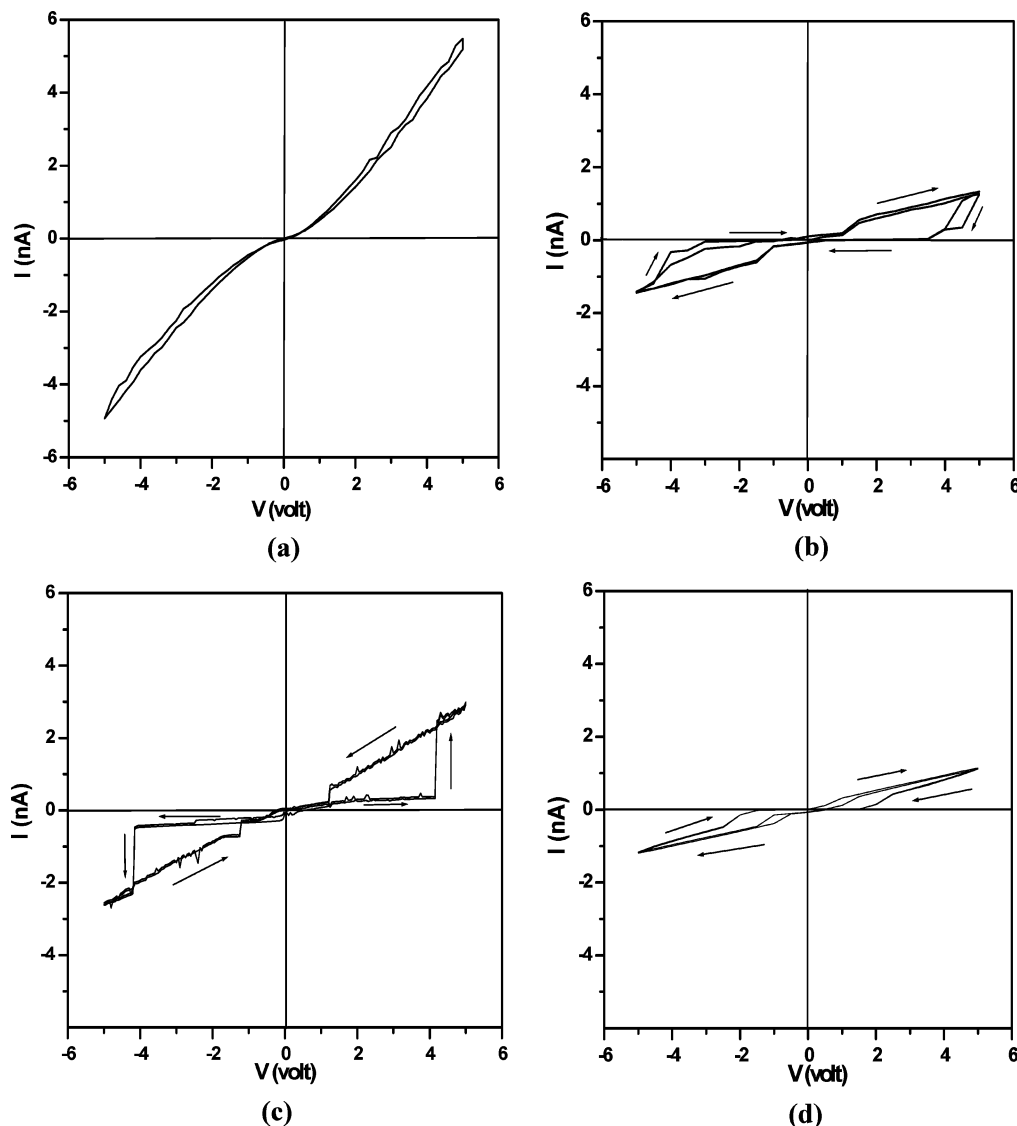
Figure 13. $I-V$ characteristics curves of PTMA and its nanoblends (a) PTMA, (b) PTMA3, (c) PTMA5, and (d) PTMA15 at 30 °C (multiple runs are shown to indicate the reversibility).

blend and the critical temperature should be below the degradation temperature of the blend. The WAXS and FTIR spectrum clearly indicates the formation of the α-polymorphic PVDF. The TGA study indicates increasing thermal stability of PVDF in the nanoblends due to the diffusion barrier property of the nanostructure. DSC study shows increasing melting and crystallization temperature of the nanoblends; the latter has been attributed to the nucleating effect of the nanophase of PTMA. The crystallinity of PVDF remains the same, and the long distance, lamellar interfacial distance, and amorphous overlayer distance decrease to different percentages. This certainly shows evidence of an attractive surface force of PTMA nanostructure in the blends. The $\pi-\pi^*$ transition band of UV–vis spectra shows a red shift with increasing PTMA concentration, and this has been attributed to the delocalization of π electrons due to the intrachain aggregation. The PL spectra of the nanoblends show a blue shift compared with that of PTMA and has been attributed to the formation of static excimer with a lower energy ground state. The lower PTMA content blends (1 and 3% w/w) show ∼8 times increase in PL intensity except 5% PTMA where interconnectivity between the nanodomains (due to spinodal decomposition) makes the nonradiative decay almost the same as in bulk PTMA. The conductivity of the nanoblends decreases

significantly as compared with that of pure PTMA and has been attributed to the twisting of the PTMA chain due to intrachin aggregation. The temperature variation of conductivity indicates a conformational transition of PTMA chain with increasing temperature facilitating better charge transport. The $I-V$ characteristic curves are really interesting; the nanoblend shows negative hysterisis except PTMA5 which shows a memory effect attributed to the electrical bistability originated from the interconnectivity of the nanophase domains during spinodal decomposition.

Supporting Information Available: ^{1}H NMR spectra of PTMA, TEM pictures of PTMA1 and PTMA15, EDXS spectra, DSC, DMA, and TGA thermograms, plot of ln σ vs 1000/T, ln W vs ln T, and $I-V$ curves of selected PTMA nanoblends.

This material is available free of charge via the Internet at http://pubs.acs.org.

References and Notes

(1) Pernot, H.; Baumert, M.; Court, F.; Leibler, L. *Nat. Mater.* **2002**, *1*, 54.

(2) Freemantle, M. *Chem. Eng. News* **2002**, *80*, 12.

(3) Kietzke, T.; Neher, D.; Landfester, K.; Montenegro, R.; Güntner, R.; Scherf, U. *Nat. Mater.* **2003**, *2*, 408.

(4) Koulic, C.; Jérôme, R. *Macromolecules* **2004**, *37*, 3459.

(5) Koulic, C.; Jérôme, R. *Macromolecules* **2004**, *37*, 888.

(6) Shimizu, H.; Li, Y.; Kaito, A.; Sano, H. *Macromolecules* **2005**, *38*, 7880.

(7) Li, Y.; Iwakura, Y.; Zhao, L.; Shimizu, H. *Macromolecules* **2008**, *41*, 3120.

(8) Mackay, M. E.; Tuteja, A.; Duxbury, P. M.; Hawker, C. J.; Horn, B. V.; Guan, Z.; Chen, G.; Krishnan, R. S. *Science* **2006**, *311*, 1740.

(9) Walther, A.; Matussek, K.; Muller, A. H. E. *ACS Nano* **2008**, *2*, 1167.

(10) Asadi, K.; De Leeuw, D. M.; Boer, B. D.; Blom, P. W. M. *Nat. Mater.* **2008**, *7*, 547.

(11) Müller, K.; Klapper, M.; Mü llen, K. *Macromol. Rapid Commun.* **2006**, *27*, 586.

(12) Li, B.; Lambeth, D. N. *Nano Lett.* **2008**, *8*, 3563.

(13) Virji, S.; Huang, J.; Kaner, R. B.; Weiller, B. H. *Nano Lett.* **2004**, *4*, 491.

(14) Huang, J.; Virji, S.; Weiller, B. H.; Kaner, R. B. *J. Am. Chem. Soc.* **2003**, *125*, 314.

(15) Huang, J.; Virji, S.; Weiller, B. H.; Kaner, R. B. *Chem.—Eur. J.* **2004**, *10*, 1314.

(16) Guo, Q.; Thomann, R.; Gronski, W.; Staneva, R.; Ivanova, R.; Stu1hn, B. *Macromolecules* **2003**, *36*, 3635.

(17) Binder, K. In *Polymers in Confined Environments*; Granik, S., Ed.; Adv. Polym. Sci, 138; Springer: Berlin, 1999.

(18) Lovinger, A. J. In *Devolepments in crystalline polymer*; Basset, D. C., Ed.; Appl. Sci.: London, 1981; Vol. 1, p 254.

(19) McCullough, R. D.; Ewbank, P. C. In *Handbook of Conducting Polymers*, 2nd ed.; Skotheim, T. A., Elsenbaumer, R. L., Reynolds, J. R., Eds.; Mercell Dekker: New York, 1998; p 225.

(20) Roerdink, E.; Challa, G. *Polymer* **1980**, *21*, 509.

(21) Belke, R. E.; Cabasso, I. *Polymer* **1988**, *29*, 8511.

(22) Maiti, P.; Nandi, A. K. *Macromolecules* **1995**, *28*, 8511.

(23) (a) Paul, D. R.; Newma, S. *Polymer Blends*; Acadamic Press: New York, 1978; Vol. I & II. (b) Olabisi, O.; Robeson, L. M.; Shaw, M. T. *Polymer -Polymer Miscibility*; Academic Press: New York, 1979.

(24) (a) Patterson, D.; Robard, A. *Macromolecules* **1978**, *11*, 690. (b) Robard, A. Ph.D. Thesis, McGill University, Canada, 1978.

(25) Cahn, J. W.; Hilliard, J. E. *J. Chem. Phys.* **1958**, *28*, 258.

(26) Cahn, J. W. *J. Chem. Phys.* **1965**, *42*, 93.

(27) Favvas, E. P.; Mitropoulos, A. C. *J. Eng. Sci. Technol. Rev.* **2008**, *1*, 25.

(28) Samanta, S.; Chatterjee, D. P.; Manna, S.; Mandal, A.; Garai, A.; Nandi, A. K. *Macromolecules* **2009**, *42*, 3112.

(29) Kim, B. S.; Chen, L.; Gong, J.; Osada, Y. *Macromolecules* **1999**, *32*, 3964.

(30) Amou, S.; Haba, O.; Shirato, K.; Hayakawa, T.; Ueda, M.; Takeuchi, K.; Asai, M. *J. Polym. Sci., Part A: Polym. Chem.* **1999**, *37*, 1943.

(31) Prest, W. M. J.; Luca, D. J. *J. Appl. Phys.* **1975**, *46*, 4136.

(32) Nandi, A. K.; Mandelkern, L. *J. Polym. Sci., Part B: Polym. Phys.* **1991**, *29*, 1287.

(33) Tompa, H. *Polymer Solutions*; Butterworths: London, 1956.

(34) Flory, P. J. *Principles of polymer chemistry*; Cornell Univ. Press: Ithaca, NY, 1953; p 541.

(35) Lando, J. B.; Doll, W. W. *J. Macromol. Sci. Phys.* **1968**, *B-2* (2), 205.

(36) Hasagawa, R.; Takahashi, Y.; Chatani, Y.; Tadokoro, H. *Polym. J.* **1972**, *3*, 600.

(37) Bachmann, M. A.; Lando, J. B. *Macromolecules* **1981**, *14*, 40.

(38) Guerra, G.; Karasz, F. E.; MacKnight, W. J. *Macromolecules* **1986**, *19*, 1935.

(39) Cortili, G.; Zerbi, G. *Spectrochim. Acta* **1967**, *23A*, 2218.

(40) Tashiro, K.; Kobayashi, M. *Phase Transitions* **1989**, *18*, 213.

(41) Manna, S.; Batabyal, S. K.; Nandi, A. K. *J. Phys. Chem. B* **2006**, *110*, 12318.

(42) Kuila, B. K.; Nandi, A. K. *Macromolecules* **2004**, *37*, 8577.

(43) Nandi, A. K. *J. Polym. Mater.* **1985**, *2*, 216.

(44) Hoffman, J. D.; Davis, G. T.; Lauritzen, J. I. J. In *Treatise on solid state chemistry*; Hannay, N. B., Ed.; Plenum Press: New York, 1976; Vol. 3, p 497.

(45) Mandelkern, L. In *Comprehensive Polymer Science*; Allen, G., Ed.; Pergamon press: Oxford, U.K., 1989; Vol. 2.

(46) Liu, Z.; Marechal, P.; Jerome, R. *Polymer* **1997**, *38*, 4925.

(47) Rughooputh, S. D. D. V.; Hotta, S.; Heeger, A. J.; Wudl, F. *J. Polym. Sci., Part B: Polym. Phys.* **1987**, *25*, 1071.

(48) Kim, S. K.; Bok, J. H.; Bartsch, R. A.; Lee, J. Y.; Kim, J. S. *Org. Lett.* **2005**, *7*, 4839.

(49) Jun, E. J.; Won, H. N.; Kim, J. S.; Lee, K. H.; Yoon, J. *Tetrahedron Lett.* **2006**, *47*, 4577.

(50) Pal, S.; Roy, S.; Nandi, A. K. *J. Phys. Chem. B* **2005**, *109*, 18332.

(51) Mennon, R.; Yoon, C. O.; Moses, D.; Heeger, A. J. In *Handbook of Conducting Polymers*, 2nd ed.; Skotheim, T. A., Elsenbaumer, R. L., Renolds, J. R., Eds.; Marcel Dekker: New York, 1998; p 27.

(52) Manna, S.; Nandi, A. K. *J. Phys. Chem. C* **2007**, *111*, 14670.

(53) Mukherjee, P.; Nandi, A. K. *J. Mater. Chem.* **2009**, *19*, 781.